

Excitation spectrum gap and spin-wave velocity of XXZ Heisenberg chains: Global renormalization-group calculation

Ozan S. Sariyer,¹ A. Nihat Berker,^{2,3,4} and Michael Hinczewski⁴

¹*Department of Physics, Istanbul Technical University, Maslak 34469, Istanbul, Turkey*

²*College of Sciences and Arts, Koç University, Sariyer 34450, Istanbul, Turkey*

³*Department of Physics, Massachusetts Institute of Technology, Cambridge, Massachusetts 02139, USA*

⁴*Feza Gürsey Research Institute, TÜBİTAK-Bosphorus University, Çengelköy 34684, Istanbul, Turkey*

(Received 9 April 2007; revised manuscript received 6 February 2008; published 4 April 2008)

The anisotropic XXZ spin- $\frac{1}{2}$ Heisenberg chain is studied using renormalization-group theory. The specific heats and nearest-neighbor spin-spin correlations are calculated throughout the entire temperature and anisotropy ranges in both ferromagnetic and antiferromagnetic regions, obtaining a global description and quantitative results. We obtain, for all anisotropies, the antiferromagnetic spin-liquid spin-wave velocity and the Ising-like ferromagnetic excitation spectrum gap, exhibiting the spin-wave to spinon crossover. A number of characteristics of purely quantum nature are found: The in-plane interaction $s_i^x s_j^x + s_i^y s_j^y$ induces an antiferromagnetic correlation in the out-of-plane s_i^z component, at higher temperatures in the antiferromagnetic XXZ chain, dominantly at low temperatures in the ferromagnetic XXZ chain, and, in-between, at all temperatures in the XY chain. We find that the converse effect also occurs in the antiferromagnetic XXZ chain: an antiferromagnetic $s_i^z s_j^z$ interaction induces a correlation in the s_i^{xy} component. As another purely quantum effect, (i) in the antiferromagnet, the value of the specific heat peak is insensitive to anisotropy and the temperature of the specific heat peak decreases from the isotropic (Heisenberg) with introduction of either type (Ising or XY) of anisotropy; and (ii) in complete contrast, in the ferromagnet, the value and temperature of the specific heat peak increase with either type of anisotropy.

DOI: [10.1103/PhysRevB.77.134413](https://doi.org/10.1103/PhysRevB.77.134413)

PACS number(s): 67.10.Fj, 75.10.Pq, 64.60.Cn, 05.10.Cc

I. INTRODUCTION

The quantum Heisenberg chain, including the possibility of spin-space anisotropy, is the simplest nontrivial quantum spin system and has thus been widely studied since the very beginning of the spin concept in quantum mechanics.¹⁻³ Interest in this model continued⁴⁻¹⁰ and redoubled with the exposition of its richly varied low-temperature behavior¹¹⁻¹³ and of its relevance to high-temperature superconductivity.¹⁴⁻¹⁸ It has become clear that antiferromagnetism and superconductivity are firmly related to each other, adjoining and overlapping each other.

A large variety of theoretical tools have been employed in the study of the various isotropic and anisotropic regimes of the quantum Heisenberg chain, including finite-systems extrapolation,^{6,19} linked-cluster⁷ and dimer-cluster²⁰ expansions, quantum decimation,²¹ decoupled Green's functions,²² quantum transfer matrix,^{23,24} high-temperature series expansion,²⁵ and numerical evaluation of multiple integrals.²⁶ The XXZ Heisenberg chain retains high current interest as a theoretical model^{27,28} with direct experimental relevance.²⁹

In the present paper, a position-space renormalization-group method introduced by Suzuki and Takano^{30,31} for $d=2$ dimensions and already applied to a number of $d>1$ systems³⁰⁻³⁶ is used to compute the spin-spin correlations and the specific heat of the $d=1$ anisotropic quantum XXZ Heisenberg model, easily resulting in a global description and detailed quantitative information for the entire temperature and anisotropy ranges including the ferromagnetic and antiferromagnetic, the spin-liquid and Ising-like regions. We obtain, for all anisotropies, the antiferromagnetic spin-liquid

spin-wave velocity and the Ising-like ferromagnetic excitation spectrum gap, exhibiting the spin-wave to spinon crossover. A number of other characteristics of purely quantum nature are found: The in-plane interaction $s_i^x s_j^x + s_i^y s_j^y$ induces an antiferromagnetic correlation in the out-of-plane s_i^z component, at higher temperatures in the antiferromagnetic XXZ chain, dominantly at low temperatures in the ferromagnetic XXZ chain, and, in-between, at all temperatures in the XY chain. We find that the converse effect also occurs in the antiferromagnetic XXZ chain: an antiferromagnetic $s_i^z s_j^z$ interaction induces a correlation in the s_i^{xy} component. As another purely quantum effect, (i) in the antiferromagnet, the value of the specific heat peak is insensitive to anisotropy and the temperature of the specific heat peak decreases from the isotropic (Heisenberg) with the introduction of either type (Ising or XY) of anisotropy; and (ii) in complete contrast, in the ferromagnet, the value of the specific heat peak is strongly dependent on anisotropy and the temperature of the specific heat peak increases with either type of anisotropy. This purely quantum effect is a precursor to different phase transition temperatures in three dimensions.^{32,36-38} Our calculational method is relatively simple, readily yields global results, and is overall quantitatively successful.

II. ANISOTROPIC QUANTUM HEISENBERG MODEL AND THE RENORMALIZATION-GROUP METHOD

A. Anisotropic quantum Heisenberg model

The spin- $\frac{1}{2}$ anisotropic Heisenberg model (XXZ model) is defined by the dimensionless Hamiltonian

$$-\beta\mathcal{H} = \sum_{\langle ij \rangle} \{J_{xy}(s_i^x s_j^x + s_i^y s_j^y) + J_z s_i^z s_j^z + G\}, \quad (1)$$

where $\beta=1/k_B T$ and $\langle ij \rangle$ denotes summation over nearest-neighbor pairs of sites. Here the s_i^μ are the quantum mechanical Pauli spin operators at site i . The additive constant G is generated by the renormalization-group transformation and is used in the calculation of thermodynamic functions. The anisotropy coefficient is $R=J_z/J_{xy}$. The model reduces to the isotropic Heisenberg model (XXX model) for $|R|=1$, to the XY model for $R=0$, and to the Ising model for $|R| \rightarrow \infty$.

B. Renormalization-group recursion relations

The Hamiltonian in Eq. (1) can be rewritten as

$$-\beta\mathcal{H} = \sum_i \{-\beta\mathcal{H}(i, i+1)\}, \quad (2)$$

where $\beta\mathcal{H}(i, i+1)$ is a Hamiltonian involving sites i and $i+1$ only. The renormalization-group procedure, which eliminates half of the degrees of freedom and keeps the partition function unchanged, is done approximately^{30,31} as

$$\begin{aligned} \text{Tr}_{\text{odd}} e^{-\beta\mathcal{H}} &= \text{Tr}_{\text{odd}} e^{\sum_i \{-\beta\mathcal{H}(i, i+1)\}} \\ &= \text{Tr}_{\text{odd}} e^{\sum_i^{\text{odd}} \{-\beta\mathcal{H}(i-1, i) - \beta\mathcal{H}(i, i+1)\}} \\ &\simeq \prod_i^{\text{odd}} \text{Tr}_i e^{\{-\beta\mathcal{H}(i-1, i) - \beta\mathcal{H}(i, i+1)\}} \\ &= \prod_i^{\text{odd}} e^{-\beta' \mathcal{H}'(i-1, i+1)} \\ &\simeq e^{\sum_i^{\text{odd}} \{-\beta' \mathcal{H}'(i-1, i+1)\}} = e^{-\beta' \mathcal{H}'}. \end{aligned} \quad (3)$$

Here and throughout this paper, the primes are used for the renormalized system. Thus at each successive length scale we ignore the noncommutativity of the operators beyond three consecutive sites, in the two steps indicated by \simeq in the above equation. Since the approximations are applied in opposite directions, one can expect some mutual compensation. Earlier studies^{30,31,33-35} have been successful in obtaining finite-temperature behavior on a variety of quantum systems.

The transformation above is summarized by

$$e^{-\beta' \mathcal{H}'(i, k)} = \text{Tr}_j e^{\{-\beta\mathcal{H}(i, j) - \beta\mathcal{H}(j, k)\}}, \quad (4)$$

where i, j, k are three successive sites. The operator $-\beta' \mathcal{H}'(i, k)$ acts on two-site states, while the operator $-\beta\mathcal{H}(i, j) - \beta\mathcal{H}(j, k)$ acts on three-site states, so that we can rewrite Eq. (4) in the matrix form

$$\langle u_i v_k | e^{-\beta' \mathcal{H}'(i, k)} | \bar{u}_i \bar{v}_k \rangle = \sum_{w_j} \langle u_i w_j v_k | e^{-\beta\mathcal{H}(i, j) - \beta\mathcal{H}(j, k)} | \bar{u}_i w_j \bar{v}_k \rangle, \quad (5)$$

where state variables u, v, w, \bar{u} , and \bar{v} can take spin-up or spin-down values at each site. The unrenormalized 8×8 matrix on the right-hand side is contracted into the renormalized 4×4 matrix on the left-hand side of Eq. (5). We use two-site basis states vectors $\{|\phi_p\rangle\}$ and three-site basis states vectors $\{|\psi_q\rangle\}$ to diagonalize the matrices in Eq. (5). The states

TABLE I. The two-site basis eigenstates that appear in Eq. (8). These are the well-known singlet and triplet states. The state $|\phi_3\rangle$ is obtained by spin reversal from $|\phi_1\rangle$, with the same eigenvalue.

p	s	m_s	Two-site basis eigenstates
+	1	1	$ \phi_1\rangle = \uparrow\uparrow\rangle$
		0	$ \phi_2\rangle = \frac{1}{\sqrt{2}}(\uparrow\downarrow\rangle + \downarrow\uparrow\rangle)$
-	0	0	$ \phi_4\rangle = \frac{1}{\sqrt{2}}(\uparrow\downarrow\rangle - \downarrow\uparrow\rangle)$

$\{|\phi_p\rangle\}$, given in Table I, are eigenstates of parity, total spin magnitude, and total spin z component. These $\{|\phi_p\rangle\}$ diagonalize the renormalized matrix, with eigenvalues

$$\Lambda_1 = \frac{1}{4}J'_z + G', \quad \Lambda_2 = +\frac{1}{2}J'_{xy} - \frac{1}{4}J'_z + G',$$

$$\Lambda_4 = -\frac{1}{2}J'_{xy} - \frac{1}{4}J'_z + G'. \quad (6)$$

The states $\{|\psi_q\rangle\}$, given in Table II, are eigenstates of parity and total spin z component. The $\{|\psi_p\rangle\}$ diagonalize the unrenormalized matrix, with eigenvalues

$$\lambda_1 = \frac{1}{2}J_z + 2G, \quad \lambda_4 = 2G,$$

$$\lambda_2 = -\frac{1}{4}(J_z + \sqrt{8J_{xy}^2 + J_z^2}) + 2G,$$

$$\lambda_3 = -\frac{1}{4}(J_z - \sqrt{8J_{xy}^2 + J_z^2}) + 2G. \quad (7)$$

With these eigenstates, Eq. (5) is rewritten as

$$\begin{aligned} \gamma_p &\equiv \langle \phi_p | e^{-\beta' \mathcal{H}'(i, k)} | \phi_p \rangle \\ &= \sum_{\substack{u, v, \bar{u}, \\ \bar{v}, w, q}} \langle \phi_p | u_i v_k \rangle \langle u_i w_j v_k | \psi_q \rangle \\ &\quad \times \langle \psi_q | e^{-\beta\mathcal{H}(i, j) - \beta\mathcal{H}(j, k)} | \psi_q \rangle \langle \psi_q | \bar{u}_i w_j \bar{v}_k \rangle \langle \bar{u}_i \bar{v}_k | \phi_p \rangle. \end{aligned} \quad (8)$$

Thus there are three independent γ_p that determine the renormalized Hamiltonian and, therefore, three renormalized in-

TABLE II. The three-site basis eigenstates that appear in Eq. (8) with coefficients $\sigma = (-J_z + \sqrt{8J_{xy}^2 + J_z^2})/2J_{xy}$, $\tau = (J_z + \sqrt{8J_{xy}^2 + J_z^2})/2J_{xy}$, and normalization factors μ, ν . The states $|\psi_{5-8}\rangle$ are obtained by spin reversal from $|\psi_{1-4}\rangle$, with the same respective eigenvalues.

p	m_s	Three-site basis eigenstates
+	3/2	$ \psi_1\rangle = \uparrow\uparrow\uparrow\rangle$
	1/2	$ \psi_2\rangle = \mu(\uparrow\uparrow\downarrow\rangle + \sigma \uparrow\downarrow\uparrow\rangle + \downarrow\uparrow\uparrow\rangle)$
		$ \psi_3\rangle = \nu(- \uparrow\uparrow\downarrow\rangle + \tau \uparrow\downarrow\uparrow\rangle - \downarrow\uparrow\uparrow\rangle)$
-	1/2	$ \psi_4\rangle = \frac{1}{\sqrt{2}}(\uparrow\downarrow\uparrow\rangle - \downarrow\uparrow\uparrow\rangle)$

teractions in the Hamiltonian closed under renormalization-group transformation, Eq. (1). These γ_p are

$$\begin{aligned}\gamma_1 &= e^{(1/4)J'_z + G'} \\ &= e^{2G - (1/4)J'_z} \left[e^{(3/4)J'_z} + \cosh\left(\frac{1}{4}\sqrt{8J_{xy}^2 + J'_z{}^2}\right) \right. \\ &\quad \left. - \frac{J'_z \sinh\left(\frac{1}{4}\sqrt{8J_{xy}^2 + J'_z{}^2}\right)}{\sqrt{8J_{xy}^2 + J'_z{}^2}} \right], \\ \gamma_2 &= e^{(1/2)J'_{xy} - (1/4)J'_z + G'} \\ &= 2e^{2G - (1/4)J'_z} \left[\cosh\left(\frac{1}{4}\sqrt{8J_{xy}^2 + J'_z{}^2}\right) \right. \\ &\quad \left. + \frac{J'_z \sinh\left(\frac{1}{4}\sqrt{8J_{xy}^2 + J'_z{}^2}\right)}{\sqrt{8J_{xy}^2 + J'_z{}^2}} \right], \\ \gamma_4 &= e^{-(1/2)J'_{xy} - (1/4)J'_z + G'} = 2e^{2G},\end{aligned}\quad (9)$$

which yield the recursion relations

$$J'_{xy} = \ln\left(\frac{\gamma_2}{\gamma_4}\right), \quad J'_z = \ln\left(\frac{\gamma_1}{\gamma_2 \gamma_4}\right), \quad G' = \frac{1}{4} \ln(\gamma_1^2 \gamma_2 \gamma_4). \quad (10)$$

As expected, J'_{xy} and J'_z are independent of the additive constant G and the derivative $\partial_G G' = b^d = 2$, where $b=2$ is the rescaling factor and $d=1$ is the dimensionality of the lattice.

For $J_{xy}=J_z$, the recursion relations reduce to the spin- $\frac{1}{2}$ isotropic Heisenberg (XXX) model recursion relations, while for $J_{xy}=0$ they reduce to the spin- $\frac{1}{2}$ Ising model recursion relations. The $J_z=0$ subspace (XY model) is not (and need not be) closed under these recursion relations:^{30,31} The renormalization-group transformation induces a positive J_z value, but the spin-space easy-plane aspect is maintained.

In addition, there exists a mirror symmetry along the J_z axis, so that $J'_{xy}(-J_{xy}, J'_z) = J'_{xy}(J_{xy}, J'_z)$ and $J'_z(-J_{xy}, J'_z) = J'_z(J_{xy}, J'_z)$. The thermodynamics of the system remains unchanged under flipping the interactions of the x and y spin components, since the renormalization-group trajectories do not change. In fact, this is part of a more general symmetry of the XYZ model, where flipping the signs of any two interactions leaves the spectrum unchanged.⁸ Therefore with no loss of generality, we take $J_{xy} > 0$. Independent of the sign of J_{xy} , $J_z > 0$ gives the ferromagnetic model and $J_z < 0$ gives the antiferromagnetic model.

C. Calculation of densities and response functions by the recursion-matrix method

Just as the interaction constants of two consecutive points along the renormalization-group trajectory are related by the

recursion relations, the densities are connected by a recursion matrix \hat{T} , which is composed of derivatives of the recursion relations. For our Hamiltonian, the recursion matrix and density vector \vec{M} are

$$\hat{T} = \begin{pmatrix} \frac{\partial G'}{\partial G} & \frac{\partial G'}{\partial J_{xy}} & \frac{\partial G'}{\partial J'_z} \\ 0 & \frac{\partial J'_{xy}}{\partial J_{xy}} & \frac{\partial J'_{xy}}{\partial J'_z} \\ 0 & \frac{\partial J'_z}{\partial J_{xy}} & \frac{\partial J'_z}{\partial J'_z} \end{pmatrix}, \quad \vec{M} = (1 \quad 2\langle s_i^{xy} s_j^{xy} \rangle \quad \langle s_i^z s_j^z \rangle). \quad (11)$$

These are densities M_α associated with each interaction K_α ,

$$M_\alpha = \frac{1}{N_\alpha} \frac{\partial \ln Z}{\partial K_\alpha}, \quad (12)$$

where N_α is the number of α -type interactions and Z is the partition function for the system, which can be expressed both via the unrenormalized interaction constants as $Z(\vec{K})$ or via the renormalized interaction constants as $Z(\vec{K}')$. By using these two equivalent forms, one can formulate the density recursion relation³⁹

$$M_\alpha = b^{-d} \sum_\beta M'_\beta T_{\beta\alpha}, \quad T_{\beta\alpha} \equiv \frac{N_\beta}{N_\alpha} \frac{\partial K'_\beta}{\partial K_\alpha}. \quad (13)$$

Since the interaction constants, under renormalization-group transformation, stay the same at fixed points such as critical fixed points or sinks, the above Eq. (13) takes the form of a solvable eigenvalue equation,

$$b^d \vec{M}^* = \vec{M}^* \cdot \hat{T}, \quad (14)$$

at fixed points, where $\vec{M} = \vec{M}' = \vec{M}^*$. The fixed point densities are the components of the left eigenvector of the recursion matrix with eigenvalue b^d .³⁹ At ordinary points, Eq. (13) is iterated until a sink point is reached under successive renormalization-group transformations. In algebraic form, this means

$$\vec{M}^{(0)} = b^{-nd} \vec{M}^{(n)} \hat{T}^{(n)} \hat{T}^{(n-1)} \dots \hat{T}^{(1)}, \quad (15)$$

where the upper indices indicate the number of iteration (transformation), with $\vec{M}^{(n)} \simeq \vec{M}^*$. This method is applied on our model Hamiltonian. The sink of the system is at infinite temperature $J_{xy}^* = J_z^* = 0$ for all initial conditions (J_{xy}, J_z) .

Response functions are calculated by differentiation of densities. For example, the internal energy is $U = -2\langle s_i^{xy} s_j^{xy} \rangle - R\langle s_i^z s_j^z \rangle$, employing $T = 1/J_{xy}$, and $U = -2\langle s_i^{xy} s_j^{xy} \rangle / R - \langle s_i^z s_j^z \rangle$, employing $T = 1/|J_z|$. The specific heat $C = \partial_T U$ follows from the chain rule,

$$C = J_{xy}^2 \frac{\partial(2\langle s_i^{xy} s_j^{xy} \rangle + R\langle s_i^z s_j^z \rangle)}{\partial J_{xy}}, \quad \text{for } T = 1/J_{xy},$$

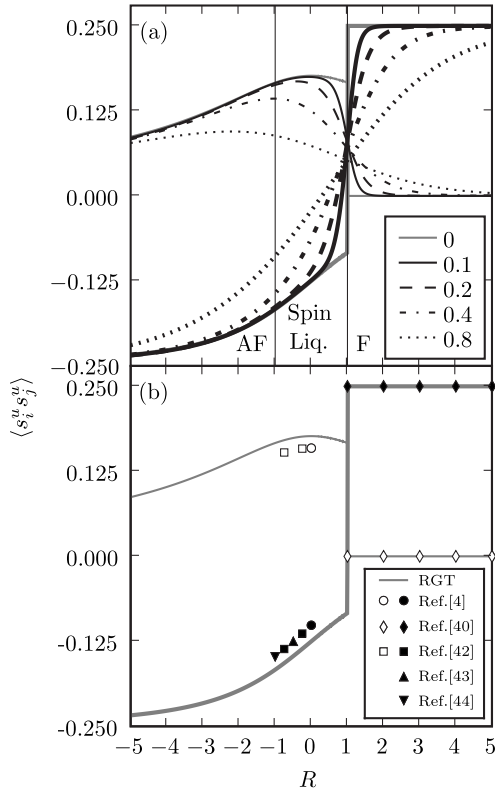


FIG. 1. (a) Calculated nearest-neighbor spin-spin correlations $\langle s_i^z s_j^z \rangle$ (thick curves from lower left) and $\langle s_i^{xy} s_j^{xy} \rangle$ (thin curves from upper left) as a function of anisotropy coefficient R for temperatures $1/J_{xy}=0, 0.1, 0.2, 0.4$, and 0.8 . (b) Calculated zero-temperature nearest-neighbor spin-spin correlations (thin and thick curves, as in the upper panel) compared with the exact points of Refs. 4, 40, and 42–44 shown with closed and open symbols for $\langle s_i^z s_j^z \rangle$ and $\langle s_i^{xy} s_j^{xy} \rangle$, respectively. At $R=1$, the calculated $\langle s_i^z s_j^z \rangle$ discontinuously goes from antiferromagnetic to the exact result of 0.25 (Ref. 40) of saturated ferromagnetism and the calculated $\langle s_i^{xy} s_j^{xy} \rangle$ discontinuously goes from ferromagnetic to the exact result of constant zero (Ref. 40).

$$C = J_z^2 \frac{\partial(2\langle s_i^{xy} s_j^{xy} \rangle / R + \langle s_i^z s_j^z \rangle)}{\partial |J_z|}, \quad \text{for } T = 1/|J_z|. \quad (16)$$

III. CORRELATIONS SCANNED WITH RESPECT TO ANISOTROPY

The ground-state and excitation properties of the XXZ model offer a variety of behaviors.^{11,12,40,41} The antiferromagnetic model with $R < -1$ is Ising-like and the ground state has Néel long-range order along the z spin component with a gap in the excitation spectrum. For $-1 \leq R \leq 1$, the system is a “spin liquid,” with a gapless spectrum and power-law decay of correlations at zero temperature. The ferromagnetic model with $R > 1$ is also Ising-like, the ground state is ferromagnetic along the z spin component, with an excitation gap.

Our calculated $\langle s_i^z s_j^z \rangle$ and $\langle s_i^{xy} s_j^{xy} \rangle \equiv \langle s_i^x s_j^x \rangle = \langle s_i^y s_j^y \rangle$ nearest-neighbor spin-spin correlations for the whole range of the anisotropy coefficient R are shown in Fig. 1 for various tem-

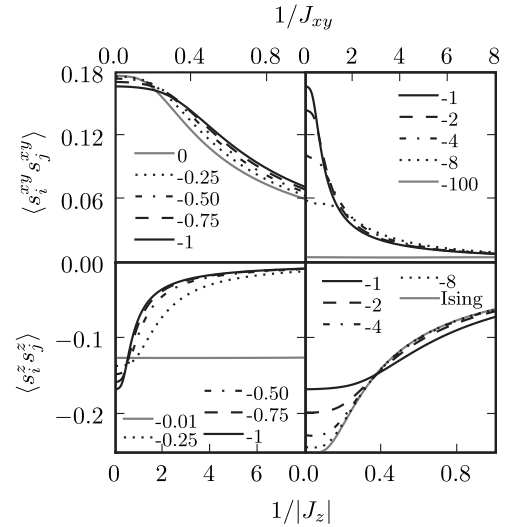


FIG. 2. Calculated nearest-neighbor spin-spin correlations $\langle s_i^{xy} s_j^{xy} \rangle$ (upper panels) and $\langle s_i^z s_j^z \rangle$ (lower panels) for the antiferromagnetic XXZ chain, as a function of temperature, for anisotropy coefficients $R=0, -0.25, -0.50, -0.75, -1, -2, -4, -8$, and $-\infty$ spanning the spin-liquid (left panels) and Ising-like (right panels) regions. Note that, in every one of the panels, the correlation curves cross each other. This remarkable quantum phenomenon is discussed in the text.

peratures. The xy correlation is always non-negative. Recall that we use $J_{xy} > 0$ with no loss of generality. In the Ising-like antiferromagnetic ($R < -1$) region, the z correlation is expectedly antiferromagnetic. As the $\langle s_i^z s_j^z \rangle$ correlation saturates for large $|R|$, the transverse $\langle s_i^{xy} s_j^{xy} \rangle$ correlation is somewhat depleted. In the Ising-like ferromagnetic ($R > 1$) region, the $\langle s_i^z s_j^z \rangle$ correlation is ferromagnetic and saturates quickly as the $\langle s_i^{xy} s_j^{xy} \rangle$ correlation quickly goes to zero. In the spin-liquid ($|R| < 1$) region, the $\langle s_i^z s_j^z \rangle$ correlation monotonically passes through zero in the ferromagnetic side, while the $\langle s_i^{xy} s_j^{xy} \rangle$ correlation is maximal. The remarkable quantum behavior of $\langle s_i^z s_j^z \rangle$ around $R=0$ is discussed in V below. It is seen in the figure that these changeovers are increasingly sharp as temperature is decreased and, at zero temperature, become discontinuous at $R=1$. As seen in Fig. 1(b), at zero temperature, our calculated $\langle s_i^z s_j^z \rangle$ and $\langle s_i^{xy} s_j^{xy} \rangle$ correlations show very good agreement with the known exact points.^{4,42–44} Also, our results for $R > 1$ fully overlap the exact results of $\langle s_i^z s_j^z \rangle = 0.25$ and $\langle s_i^{xy} s_j^{xy} \rangle = 0$.⁴⁰ We also note that zero temperature is the limit in which our approximation is at its worst.

IV. ANTIFERROMAGNETIC XXZ CHAIN

For the antiferromagnetic XXZ chain, our calculated $\langle s_i^z s_j^z \rangle$ and $\langle s_i^{xy} s_j^{xy} \rangle$ nearest-neighbor spin-spin correlations as a function of temperature are shown in Fig. 2 for various anisotropy coefficients R . We find that when J_{xy} is the dominant interaction (spin liquid), the correlations are weakly dependent on anisotropy R . When J_z is the dominant interaction (Ising-like), the correlations are weakly dependent on anisotropy R only at the higher temperatures. Our results are com-

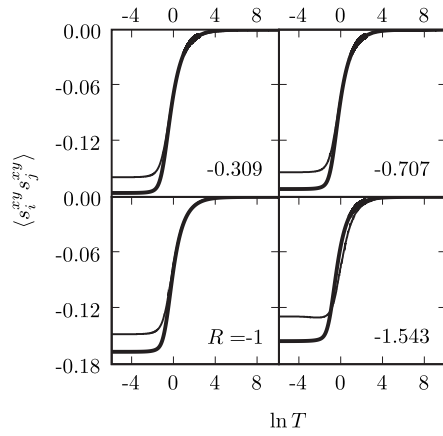


FIG. 3. Comparison of our results (thick lines) for the correlation functions of the antiferromagnetic XXZ chain, with the multiple-integral results of Ref. 26 (thin lines), for various anisotropy coefficients R spanning the spin-liquid and Ising-like regions.

pared with multiple-integral results²⁶ in Fig. 3.

In every one of the panels of Fig. 2, the correlation curves cross each other, revealing a remarkable quantum phenomenon. In a classical system, the correlation between a given spin component (e.g., $\langle s_i^{xy} s_j^{xy} \rangle$) is expected to decrease when the coupling of another spin component (e.g., $|J_z|$) is increased. It is found from the antiferromagnetic XXZ chain in Fig. 2 that the opposite may occur in a quantum system: In this figure, an increase in J_{xy} causes an increase in $|\langle s_i^z s_j^z \rangle|$ for $1/|J_z| > 0.9$ and 0.4 in the spin-liquid and Ising-like regions, respectively. Conversely, an increase in $|J_z|$ causes an increase in $\langle s_i^{xy} s_j^{xy} \rangle$ for $1/J_{xy} > 0.4$ and 2.1 in the spin-liquid and Ising-like regions, respectively. This quantum effect can be called cross-component spin correlation.

The antiferromagnetic specific heats calculated with Eq. (16) are shown in Fig. 4 for various anisotropy coefficients and compared, in Figs. 5 and 6, with finite-lattice

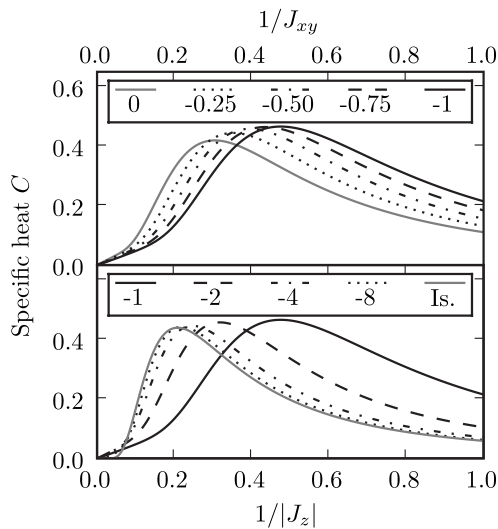


FIG. 4. Calculated specific heats C of the antiferromagnetic XXZ chain, as a function of temperature for anisotropy coefficients $R=0, -0.25, -0.50, -0.75, -1, -2, -4, -8,$ and $-\infty$ spanning the spin-liquid (upper panel) and Ising-like (lower panel) regions.

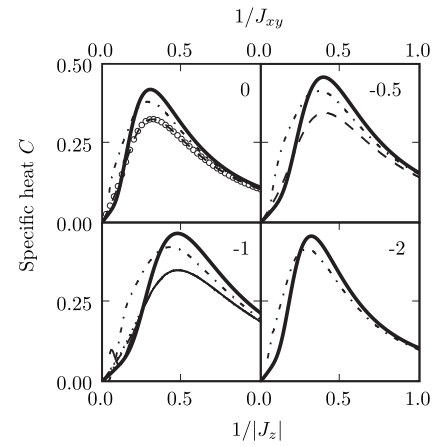


FIG. 5. Comparison of our antiferromagnetic specific heat results (thick lines) with the results of Refs. 5 (open circles), Ref. 6 (dotted line), Ref. 19 (thin line), Ref. 21 (dash-dotted lines), and Refs. 23 and 24 (dashed lines), for anisotropy coefficients $R=0, -0.5, -1,$ and -2 spanning the spin-liquid and Ising-like regions.

expansion,^{6,19} quantum decimation,²¹ transfer matrix,²⁴ high-temperature series expansion²⁵ results and, for the $R=0$ case, namely the XY model, with the exact result⁵ $C = (1/4\pi T) \int_0^\pi [\cos \omega / \cosh(\frac{\cos \omega}{2T})]^2 d\omega$. The $C(T)$ peak temperature is highest for the isotropic case (Heisenberg) and decreases with anisotropy increasing in either direction (towards Ising or XY). The peak value of $C(T)$ is only weakly dependent on anisotropy, especially for the Ising-like systems. A strong contrast to this behavior will be seen, as another quantum mechanical phenomenon, in the ferromagnetic XXZ chain.

The linearity, at low temperatures, of the spin liquid ($|R| \leq 1$) specific heat with respect to temperature is expected on the basis of spin-wave calculations for the antiferromagnetic XXZ model.^{45,46} This linear form of $C(T)$ reflects the linear energy-momentum dispersion of the low-lying excitations, the magnons. The low-temperature magnon dispersion relation is $\hbar\omega = ck^n$, where c is the spin-wave velocity and $n=1$ for the antiferromagnetic XXZ model in $d=1$.⁴⁰ The internal energy, given by $U = (1/2\pi) \int_0^\infty dk \hbar\omega(k) / (e^{\beta\hbar\omega(k)} - 1)$, is dominated by the magnons at low temperatures, yielding $U \sim T^2$ and $C \sim T$ for $n=1$ in the dispersion relation. From this relation, our calculated spin-wave velocity c as a function of anisotropy R is given in Fig. 7 and compares well with the also shown exact result.⁴⁷ A simultaneous fit to the dispersion relation exponent n , expected to be 1, yields 1.00 ± 0.02 . However, for the Ising-like $-R > 1$, the unexpected linearity instead of an exponential form caused by a gap in the excitation spectrum points to the approximate nature of our renormalization-group calculation. The correct exponential form is obtained in the large $-R$ limit, where the renormalization-group calculation becomes exact.

Rojas *et al.*²⁵ have obtained the high-temperature expansion of the free energy of the XXZ chain to order β^3 , where β is the inverse temperature. The specific heat from this expansion is

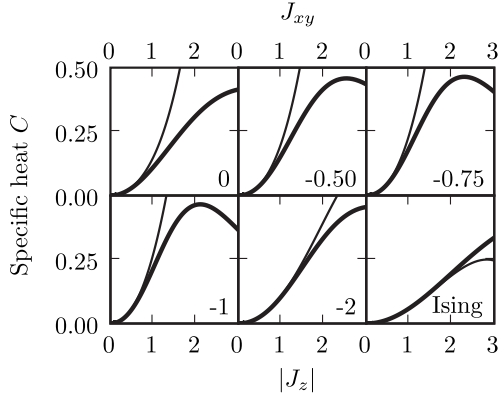


FIG. 6. Comparison of our antiferromagnetic specific heat results (thick lines) with the high-temperature $J \rightarrow 0$ behaviors (thin lines) obtained from series expansion in Ref. 25 for anisotropy coefficients $R=0, -0.50, -0.75, -1, -2,$ and $-\infty$ spanning the spin-liquid and Ising-like regions.

$$C = \frac{2+R^2}{16} J_{xy}^2 - \frac{3R}{32} J_{xy}^3 + \frac{6-8R^2-R^4}{256} J_{xy}^4. \quad (17)$$

This high-temperature specific heat result is also compared with our results, in Fig. 6, and very good agreement is seen. In fact, when in the high-temperature region of $0 < \beta < 0.1$, we fit our numerical results for $C(\beta)$ to the fourth degree polynomial $C = \sum_{i=0}^4 A_i \beta^i$, and we do find (1) the vanishing $A_0 < 10^{-5}$ and $A_1 < 10^{-7}$ for all R and (2) the comparison in Fig. 8 between our results for A_2 and A_3 and those of Eq. (17) from Ref. 25, thus obtaining excellent agreement for all regions of the model.

V. FERROMAGNETIC XXZ CHAIN

For the ferromagnetic (i.e., $R > 0$) systems in Fig. 1, the $\langle s_i^z s_j^z \rangle$ expectation value becomes rapidly negative at lower temperatures for $R < 1$, even though for $R \geq 0$ all couplings in the Hamiltonian are ferromagnetic. This is actually a real physical effect, not a numerical anomaly. In fact, we know

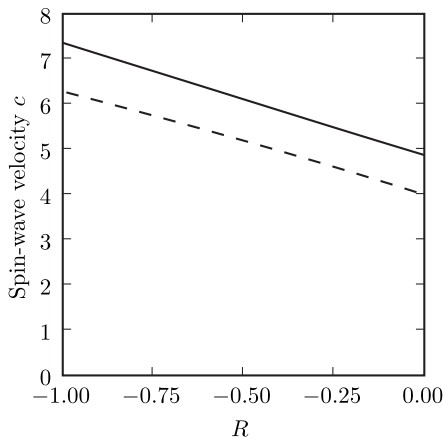


FIG. 7. Our calculated antiferromagnetic spin-wave velocity c versus the anisotropy coefficient R . The dashed line, $2\pi \sin(\gamma)/\gamma$ where $\gamma \equiv \cos^{-1}(-R)$, is the exact result (Ref. 47).

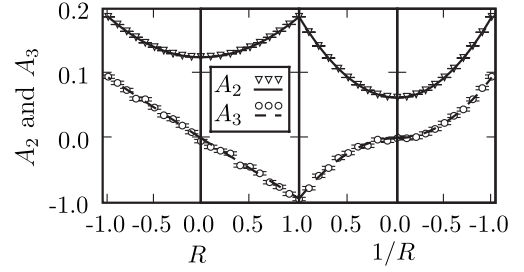


FIG. 8. Comparison of our results with the high-temperature expansion of Ref. 25 for all regions: antiferromagnetic (outer panels) and ferromagnetic (inner panels), spin-liquid (left panels) and Ising-like (right panels). Triangles and circles denote our results, while solid and dashed lines denote the results of Ref. 25 for A_2 and A_3 , respectively. The error bars, due to the statistical fitting procedure of the coefficients A_2 and A_3 , have half-heights of 1.7×10^{-4} and 2.6×10^{-3} , respectively.

the spin-spin correlations for the ground state of the one-dimensional XY model (the $R=0$ case of our Hamiltonian), and we can compare our low-temperature results with these exact values. The ground-state properties of the spin- $\frac{1}{2}$ XY model are studied by making a Jordan-Wigner transformation, yielding a theory of noninteracting spinless fermions. Analysis of this theory yields the exact zero-temperature nearest-neighbor spin-spin correlations⁴ shown in Table III. Our renormalization-group results in the zero-temperature limit, also shown in this table, compare quite well with the exact results, as with the other exact points in Fig. 1(b), although in the worst region for our approximation. Finally, by continuity, it is reasonable that for a range of R positive but less than one, the z component correlation function is as we find, intriguingly but correctly negative at low temperatures. Thus the interaction $s_i^x s_j^x + s_i^y s_j^y$ (irrespective of its sign, due to the symmetry mentioned at the end of Sec. II B) induces an antiferromagnetic correlation in the s_i^z component, competing with the $s_i^z s_j^z$ interaction when the latter is ferromagnetic.

For finite temperatures, our calculated nearest-neighbor spin-spin correlations are shown in Figs. 9 and 10 for different values of R . These results are compared with Green's function calculations²² in Fig. 11. As expected from the discussion at the beginning of this section, in the spin-liquid region, the correlation $\langle s_i^z s_j^z \rangle$ is negative at low temperatures. Thus a competition occurs in the correlation $\langle s_i^z s_j^z \rangle$ between the XY -induced antiferromagnetism and the ferromagnetism due to the direct coupling between the s^z spin components. In

TABLE III. Zero-temperature nearest-neighbor correlations of the spin- $\frac{1}{2}$ XY chain.

Zero-temperature correlations of the spin- $\frac{1}{2}$ XY chain	Exact values from Ref. 4	Our renormalization-group theory results
$\langle s_i^{xy} s_j^{xy} \rangle$	0.15915	0.17678
$\langle s_i^z s_j^z \rangle$	-0.10132	-0.12500

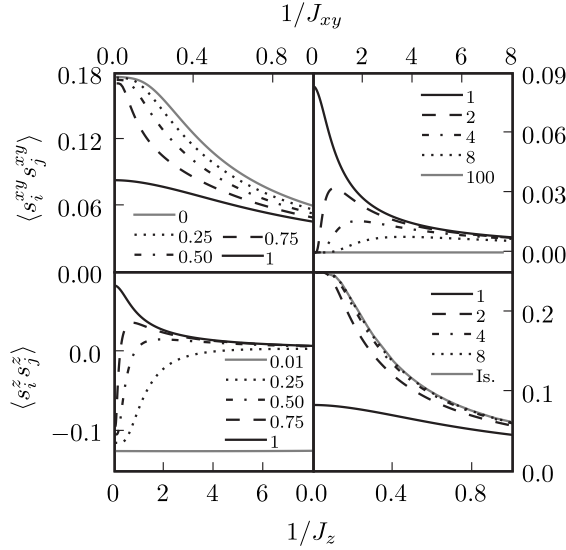


FIG. 9. Calculated nearest-neighbor spin-spin correlations $\langle s_i^{xy} s_j^{xy} \rangle$ (upper panels) and $\langle s_i^z s_j^z \rangle$ (lower panels) for the ferromagnetic XXZ chain, as a function of temperature, for anisotropy coefficients $R=0, 0.25, 0.50, 0.75, 1, 2, 4, 8$, and ∞ spanning the spin-liquid (left panels) and Ising-like (right panels) regions.

fact, the reinforcement of antiferromagnetic correlations of $\langle s_i^z s_j^z \rangle$ by increasing J_{xy} (and also its converse) was seen in the antiferromagnetic XXZ chain discussed in the previous section. Thus we see that whereas this cross-component effect is dominant at low temperatures in the ferromagnetic XXZ chain, it is seen at higher temperatures in the antiferromagnetic XXZ chain and, in-between, throughout the temperature range in the XY chain.

In the ferromagnetic XXZ chain, as a consequence of the competition mentioned above, a sign reversal in $\langle s_i^z s_j^z \rangle$ occurs from negative to positive correlation, at temperatures $J_{xy}^{-1} = T_0(R)$.⁴⁸ At this temperature, by cancellation of the competing effects, the nearest-neighbor correlation $\langle s_i^z s_j^z \rangle$ is zero. Our calculated $T_0(R)$ curve is shown in Fig. 10 and has very good agreement with the exact result $T_0 = (\sqrt{3} \sin \gamma / 4 \gamma) \tan[\pi(\pi - \gamma) / 2 \gamma]$ where $\gamma \equiv \cos^{-1}(-R)$.²³

The calculated ferromagnetic specific heats are shown in Fig. 12 for various anisotropy coefficients and compared, in

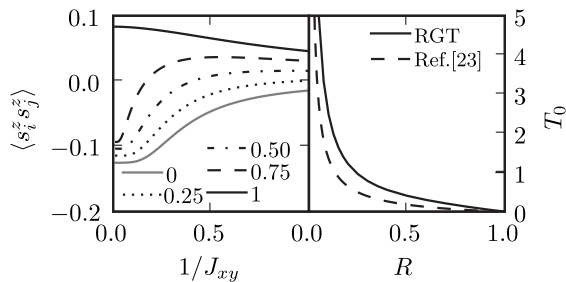


FIG. 10. Left panel: Calculated nearest-neighbor spin-spin correlations $\langle s_i^z s_j^z \rangle$ for the ferromagnetic XXZ chain, as a function of temperature $1/J_{xy}$ in the spin liquid, for anisotropy coefficients $R=0, 0.25, 0.50, 0.75$, and 1 . Right panel: The sign-reversal temperature T_0 of the nearest-neighbor correlation $\langle s_i^z s_j^z \rangle$: our results (full curve) and the analytical result from the quantum transfer matrix method (dashed) (Ref. 23).

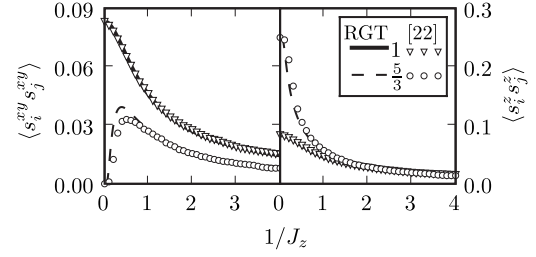


FIG. 11. Comparison of our ferromagnetic $R=1, \frac{5}{3}$ results with Green's function calculations (Ref. 22).

Figs. 13 and 14, with finite-lattice expansion,⁶ quantum decimation,²¹ decoupled Green's functions,²² transfer matrix,^{23,24} high-temperature series expansion²⁵ results and, for the $R=0$ case, namely the XY model, with the exact result⁵ $C = (1/4 \pi T) \int_0^\pi [\cos \omega / \cosh(\frac{\cos \omega}{2T})]^2 d\omega$. In sharp contrast to the antiferromagnetic case in Sec. IV, the peak $C(T)$ temperature is highest for the most anisotropic cases (XY or Ising) and decreases with anisotropy decreasing from either direction (towards Heisenberg). In the same contrast, the peak value of $C(T)$ is dependent on anisotropy, decreasing, eventually to a flat curve, as anisotropy is decreased. This contrast between the ferromagnetic and antiferromagnetic systems is a purely quantum phenomenon. Specifically, the marked contrast between the specific heats of the isotropic antiferromagnetic and ferromagnetic systems, seen in the full curves of Figs. 4 and 12 respectively, translates into the different critical temperatures of the respective three-dimensional systems.^{32,36-38} Classical ferromagnetic and antiferromagnetic systems are, on the other hand, identically mapped onto each other.

The low-temperature specific heats are discussed in detail and compared to other results in Sec. VI.

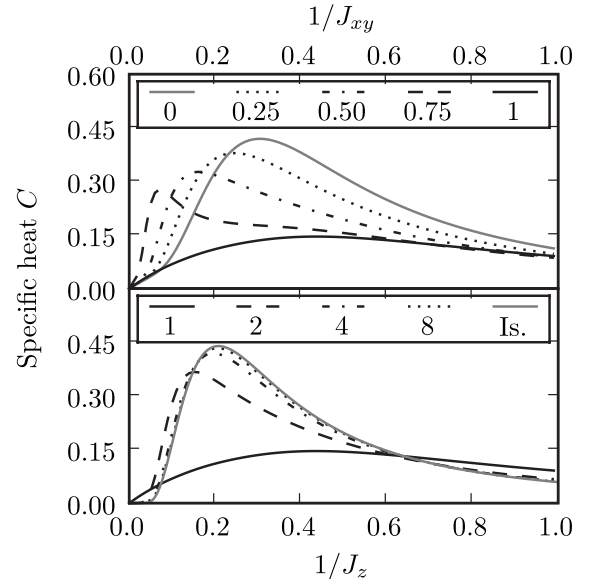


FIG. 12. Calculated specific heats C of the ferromagnetic XXZ chain, as a function of temperature for anisotropy coefficients $R=0, 0.25, 0.50, 0.75, 1, 2, 4, 8$, and ∞ spanning the spin-liquid (upper panel) and Ising-like (lower panel) regions.

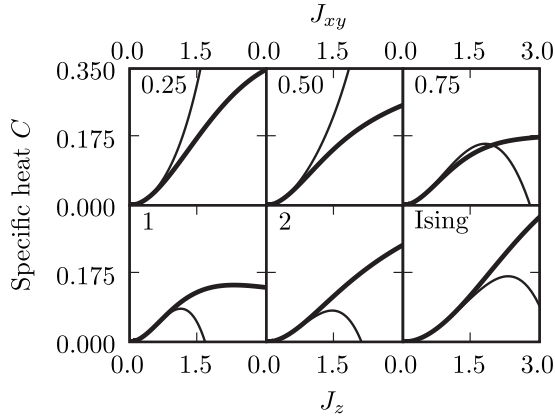


FIG. 13. Comparison of our ferromagnetic specific heat results (thick lines) with the high-temperature $J \rightarrow 0$ behaviors (thin lines) obtained from series expansion (Ref. 25), for anisotropy coefficients $R=0.25, 0.50, 0.75, 1, 2,$ and ∞ spanning the spin-liquid and Ising-like regions.

VI. LOW-TEMPERATURE SPECIFIC HEATS

Properties of the low-temperature specific heat of the ferromagnetic XXZ chain have been derived from the thermodynamic Bethe-ansatz equations.⁴⁰ For anisotropy coefficient $|R| \leq 1$, the model is gapless^{11,12} and, except at $R=1$, the specific heat is linear in $T=J_{xy}^{-1}$ in the zero-temperature limit, $C/T=2\gamma/(3 \sin \gamma)$ where again $\gamma = \cos^{-1}(-R)$. Note that this result contradicts the spin-wave theory prediction of $C \sim T^{1/2}$ for the ferromagnetic chain ($n=2$ for the ferromag-

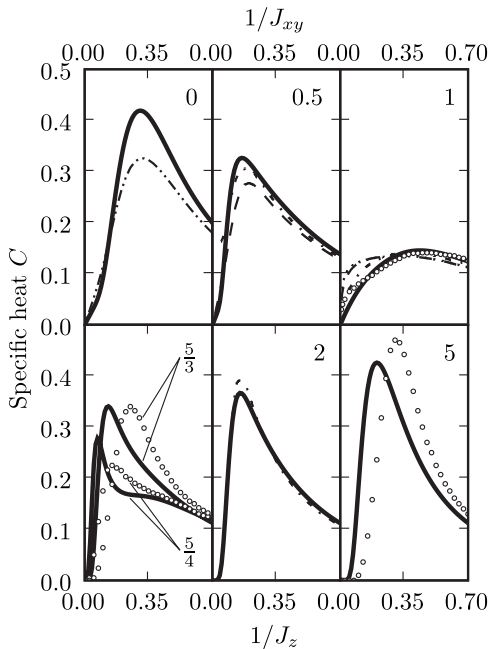


FIG. 14. Comparison of our ferromagnetic specific heat results (thick lines) with the results of Ref. 5 (dash-double-dotted line), Ref. 6 (dotted line), Ref. 21 (dash-dotted lines), Ref. 22 (open circles), and Refs. 23 and 24 (dashed lines), for anisotropy coefficients $R=0, 0.5, 1, \frac{5}{4}, \frac{5}{3}, 2,$ and 5 spanning the spin-liquid and Ising-like regions.

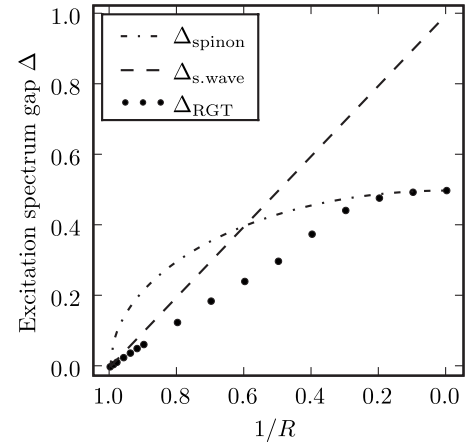


FIG. 15. The calculated excitation spectrum gap Δ versus anisotropy.

netic magnon dispersion relation of the kind given above in Sec. IV). The spin-wave result is valid only for $R=1$, the isotropic Heisenberg case. From the expression given above, we see that C/T diverges as $R \rightarrow 1^-$, and at exactly $R=1$ it has been shown that $C \sim T^{1/2}$.⁴⁰

In the Ising-like region $R > 1$, the system exhibits a gap in its excitation spectrum and the specific heat behaves as $C \sim T^{-a} \exp(-\Delta/T)$, with Δ being the excitation spectrum gap.^{11,12,40} There exist two gaps for the energy, called the spinon gap and the spin-wave gap, given by $\Delta_{\text{spinon}} = \frac{1}{2}\sqrt{1-R^2}$ and $\Delta_{\text{spin wave}} = 1-R^{-1}$. These are the minimal energies of elementary excitations.^{10,40} A crossover between them occurs at $R = \frac{5}{3}$: below this value, the spinon gap is lower, while above this value the spin-wave gap is lower. We have double-fitted our calculated specific heats with respect to the gap Δ and the leading exponent a , for the entire range of anisotropy R between $0 < R^{-1} < 1$ (Fig. 15). Our calculated gap Δ behaves linearly in R^{-1} for R^{-1} close to 1, and crosses over to $1/2$ at $R^{-1}=0$, as expected. We also obtain the exponent $a=1.99 \pm 0.02$ in the Ising limit $R^{-1} \leq 0.2$ and $a=1.52 \pm 0.10$ in the Heisenberg limit $R^{-1} \geq 0.9$. These exponent values are, respectively, expected to be 2 and 1.5.^{9,10}

We now turn to the discussion of our specific heat results for the entire ferromagnetic and antiferromagnetic ranges. Our calculated C/T curves are plotted as a function of anisotropy and temperature in Figs. 16 and 17, respectively. We discuss each region of the anisotropy R separately.

(i) $R > 1$: The specific heat coefficient C/T vanishes in the $T \rightarrow 0$ limit and has the expected exponential form as discussed above in this section. The spin-wave to spinon excitation gap crossover is obtained.

(ii) $R \approx 1$: The double-peak structure of C/T in Fig. 16 is centered at $R=1$. As temperature goes to zero, the peaks narrow and diverge.

(iii) $-1 \leq R < 1$: The specific heat coefficient is $C/T = 2\gamma/(3 \sin \gamma)$ in this region,^{11,40} and our calculated specific heat is indeed linear at low temperatures. The C/T curves for $R=-1, -0.5,$ and 0.5 in Fig. 17 all extrapolate to nonzero limits at $T=0$. The spin-wave dispersion relation exponent and velocity, for the antiferromagnetic system, is correctly obtained for the isotropic case and for all anisotropies, as

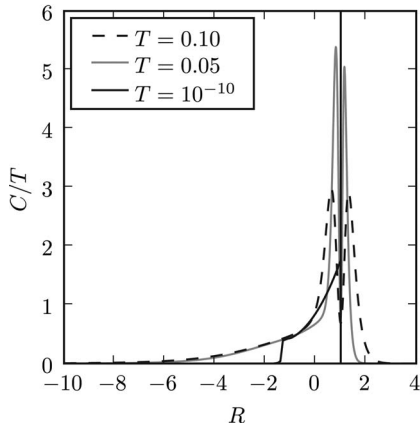


FIG. 16. Calculated specific heat coefficient C/T as a function of anisotropy R , for $T=0.10, 0.05, 10^{-10}$.

seen in Fig. 7. Figure 18 directly compares $C/T = 2\gamma/(3 \sin \gamma)$ with our results: The curves have the same basic form, gradually rising from $R=-1$, with a sharp divergence as R nears 1. At $R=1^+$, we expect $C/T=0$. Our $T=10^{-10}$ curve diverges at $R=1$ and indeed returns to zero at $R=1.000\,000\,1$.

(iv) $R < -1$: We expect a vanishing C/T , which we do find as seen in Fig. 16 and in the insets of Fig. 17. The exponential behavior of the specific heat is clearly seen in the Ising limit.

VII. CONCLUSION

A detailed global renormalization-group solution of the XXZ Heisenberg chain, for all temperatures and anisotropies, for both ferromagnetic and antiferromagnetic couplings, has

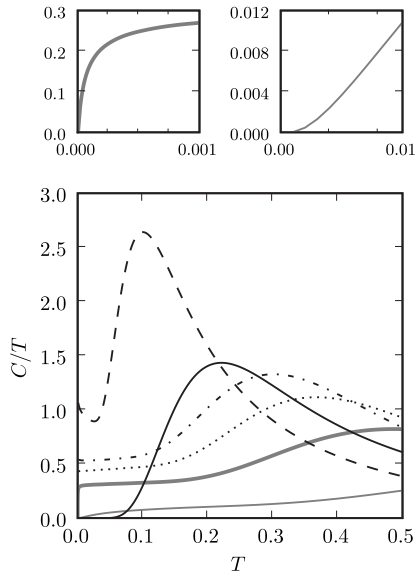


FIG. 17. Calculated specific heat coefficient C/T as a function of temperature for anisotropy coefficient $R=-5$ (thin gray line), $R=-2$ (thick gray line), -1 (dotted line), -0.5 (dash-dotted line), 0.5 (dashed line), and 2 (thin black line).

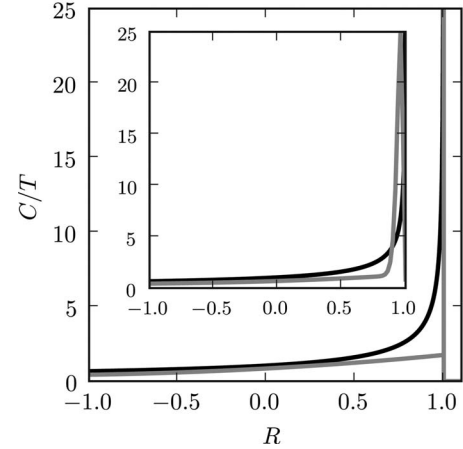


FIG. 18. Calculated specific heat coefficient C/T as a function of anisotropy coefficient R in the spin-liquid region, $-1 \leq R \leq 1$, at constant temperature $T=10^{-10}$. Our renormalization-group result (gray curve) is compared to the zero-temperature Bethe-ansatz result (black curve). Inset: our calculation (gray curve) at constant $T=10^{-2}$ is again compared to the zero-temperature Bethe-ansatz result (black curve).

been obtained. In the spin-liquid region, the linear low-temperature specific heat and, for the antiferromagnetic chain, the spin-wave dispersion relation exponent n and velocity c have been obtained. In the Ising-like region, the spin-wave to spinon crossover of the excitation spectrum gap of the ferromagnetic chain has been obtained from the exponential specific heat, as well as the correct leading algebraic behaviors in the Heisenberg and Ising limits. Purely quantum mechanical effects have been seen: We find that the xy correlations and the antiferromagnetic z correlations mutually reinforce each other, for different ranges of temperatures and anisotropies, in ferromagnetic, antiferromagnetic, and XY systems. The behaviors, with respect to anisotropy, of the specific heat peak values and locations are opposite in the ferromagnetic and antiferromagnetic systems. The sharp contrast found in the specific heats of the isotropic ferromagnetic and antiferromagnetic systems is a harbinger of the different critical temperatures in the respective three-dimensional systems. When compared with existing calculations in the various regions of the global model, good quantitative agreement is seen. Even at zero temperature, where our approximation is at its worst, good quantitative agreement is seen with exact data points for the correlation functions [Fig. 1(b)], which we extend to all values of the anisotropy. Finally, the relative ease with which the Suzuki-Takano decimation procedure is globally and quantitatively implemented should be noted.

ACKNOWLEDGMENTS

This research was supported by the Scientific and Technological Research Council (TÜBİTAK) and by the Academy of Sciences of Turkey. One of us (O.S.S.) gratefully acknowledges support from the Turkish Scientific and Technological Research Council–Scientist Training Group (TÜBİTAK-BAYG).

- ¹F. Bloch, Z. Phys. **61**, 206 (1930).
²H. Bethe, Z. Phys. **71**, 205 (1931).
³L. Hulthén, Ark. Mat., Astron. Fys. **26**, 1 (1938).
⁴E. Lieb, T. Schultz, and D. Mattis, Ann. Phys. (N.Y.) **16**, 407 (1961).
⁵S. Katsura, Phys. Rev. **127**, 1508 (1962).
⁶J. C. Bonner and M. E. Fisher, Phys. Rev. **135**, A640 (1964).
⁷S. Inawashiro and S. Katsura, Phys. Rev. **140**, A892 (1965).
⁸C. N. Yang and C. P. Yang, Phys. Rev. **147**, 303 (1966).
⁹J. D. Johnson and J. C. Bonner, Phys. Rev. Lett. **44**, 616 (1980).
¹⁰J. D. Johnson and J. C. Bonner, Phys. Rev. B **22**, 251 (1980).
¹¹F. D. M. Haldane, Phys. Rev. Lett. **45**, 1358 (1980).
¹²F. D. M. Haldane, Phys. Rev. B **25**, 4925 (1982).
¹³F. D. M. Haldane, Phys. Lett. **93A**, 464 (1983).
¹⁴J. G. Bednorz and K. A. Müller, Z. Phys. B: Condens. Matter **64**, 189 (1986).
¹⁵E. Manousakis, Rev. Mod. Phys. **63**, 1 (1991), and references therein.
¹⁶B. Keimer, N. Belk, R. J. Birgeneau, A. Cassanho, C. Y. Chen, M. Greven, M. A. Kastner, A. Aharony, Y. Endoh, R. W. Erwin, and G. Shirane, Phys. Rev. B **46**, 14034 (1992).
¹⁷M. Greven, R. J. Birgeneau, Y. Endoh, M. A. Kastner, M. Matsuda, and G. Shirane, Z. Phys. B: Condens. Matter **96**, 465 (1995).
¹⁸R. J. Birgeneau, A. Aharony, N. R. Belk, F. C. Chou, Y. Endoh, M. Greven, S. Hosoya, M. A. Kastner, C. H. Lee, Y. S. Lee, G. Shirane, S. Wakimoto, B. O. Wells, and K. Yamada, J. Phys. Chem. Solids **56**, 1913 (1995).
¹⁹R. Narayanan and R. R. P. Singh, Phys. Rev. B **42**, 10305 (1990).
²⁰M. Karbach, K. H. Mütter, P. Ueberholz, and H. Kröger, Phys. Rev. B **48**, 13666 (1993).
²¹Chen Xi-Yao and G. F. Tuthill, Phys. Rev. B **32**, 7280 (1985).
²²W. J. Zhang, J. L. Shen, J. H. Xu, and C. S. Ting, Phys. Rev. B **51**, 2950 (1995).
²³K. Fabricius, A. Klümper, and B. M. McCoy, in *Statistical Physics on the Eve of the 21st Century*, edited by M. T. Batchelor and L. T. Wille (World Scientific, Singapore 1999), p. 351.
²⁴A. Klümper, *Integrability of Quantum Chains: Theory and Applications to the Spin-1/2 XXZ Chain*, Lecture Notes in Physics Vol. 645 (Springer, Berlin, 2004), p. 349.
²⁵O. Rojas, S. M. de Souza, and M. T. Thomaz, J. Math. Phys. **43**, 1390 (2002).
²⁶M. Bortz and F. Göhman, Eur. Phys. J. B **46**, 399 (2005).
²⁷J. Damerau, F. Göhman, N. P. Hasenclever, and A. Klümper, J. Phys. A **40**, 4439 (2007).
²⁸A. Y. Hu, Y. Chen, and L. J. Peng, J. Magn. Magn. Mater. **313**, 366 (2007).
²⁹S. Thanos, Physica A **378**, 273 (2007).
³⁰M. Suzuki and H. Takano, Phys. Lett. **69A**, 426 (1979).
³¹H. Takano and M. Suzuki, J. Stat. Phys. **26**, 635 (1981).
³²A. Falicov and A. N. Berker, Phys. Rev. B **51**, 12458 (1995).
³³P. Tomczak, Phys. Rev. B **53**, R500 (1996).
³⁴P. Tomczak and J. Richter, Phys. Rev. B **54**, 9004 (1996).
³⁵P. Tomczak and J. Richter, J. Phys. A **36**, 5399 (2003).
³⁶M. Hinczewski and A. N. Berker, Eur. Phys. J. B **48**, 1 (2005).
³⁷G. S. Rushbrooke and P. J. Wood, Mol. Phys. **6**, 409 (1963).
³⁸J. Oitmaa and W. Zheng, J. Phys.: Condens. Matter **16**, 8653 (2004).
³⁹S. R. McKay and A. N. Berker, Phys. Rev. B **29**, 1315 (1984).
⁴⁰M. Takahashi, *Thermodynamics of One-Dimensional Solvable Models* (Cambridge University Press, Cambridge, England 1999), pp. 41, 56, 152–158, and references therein.
⁴¹D. V. Dmitriev, V. Ya. Krivnov, and A. A. Ovchinnikov, Phys. Rev. B **65**, 172409 (2002).
⁴²G. Kato, M. Shiroishi, M. Takahashi, and K. Sakai, J. Phys. A **37**, 5097 (2004).
⁴³N. Kitane, J. M. Maillet, N. A. Slavnov, and V. Terras, J. Stat. Mech.: Theory Exp. (2005) L09002.
⁴⁴J. Sato, M. Shiroishi, and M. Takahashi, Nucl. Phys. B **729**, 441 (2005).
⁴⁵R. Kubo, Phys. Rev. **87**, 568 (1952).
⁴⁶J. Van Kranendonk and J. H. Van Vleck, Rev. Mod. Phys. **30**, 1 (1958).
⁴⁷J. des Cloizeaux and M. Gaudin, J. Math. Phys. **7**, 1384 (1966).
⁴⁸C. Schindelin, H. Fehske, H. Büttner, and D. Ihle, Phys. Rev. B **62**, 12141 (2000).